THE JOURNAL OF PHYSICAL CHEMISTRY A

Article

pubs.acs.org/JPCA

# Ground and Electronically Excited Singlet State Structures of the *syn* and *anti* Rotamers of 5-Hydroxyindole

Olivia Oeltermann, Christian Brand, Martin Wilke, and Michael Schmitt*

Heinrich-Heine-Universität Institut für Physikalische Chemie, I D-40225 Düsseldorf, Germany

Supporting Information

**ABSTRACT:** The electronic origin bands A and B of 5-hydroxyindole were measured using rotationally resolved electronic spectroscopy. From comparison of the experimental rotational constants to the results of ab initio calculated structures, we could make the assignment of band A being due to the *syn* conformer and of band B being due to the *anti* conformer. These conformers, which differ in the orientation of the hydroxy group with respect to the rest of the molecule, have considerably different $S_1$ state life times. The most probable explanation for this surprising finding is a different conical intersection of the $\pi\pi^*$ states of both conformers with the repulsive $\pi\sigma^*$ state.

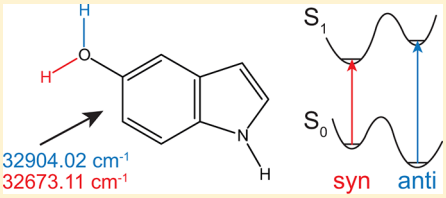


## 1. INTRODUCTION

5-Hydroxyindole (5OHI) is the chromophore of serotonin (5-hydroxytryptamine), which acts both as hormone and neurotransmitter.

R2PI spectra taken by Arnold and Sulkes[1] and by Huang and Sulkes[2] showed two origin bands at 32 685 $cm^{-1}$ and at 32 914 $cm^{-1}$, which can be attributed to two conformers of 5OHI. They are due to the different positions of the hydroxy group, with respect to the asymmetric frame of the molecule and are called *syn* and *anti* (cf. Figure 1).

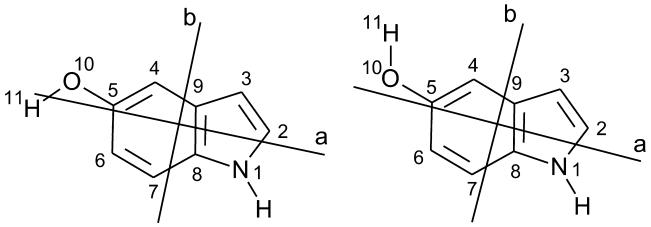


**Figure 1.** Atomic numbering and orientation of the inertial axes *syn*- and *anti*-5OHI.

A study on dynamics of electronic relaxation in gas-phase 5-hydroxyindole following UV excitation with femtosecond laser pulses has been presented by Livingstone.[3] H atom photofragment translational spectroscopy (HRA-PTS) has been used in the Ashfold group, to explore the competing NH and OH bond dissociation pathways of 5-hydroxyindole.[4] Catalan et al.[5] presented a CNDO/S study on the lowest excited singlet states in 5OHI. A combined ab initio (CASPT2) and absorption and emission spectroscopic study on 5-hydroxyindole in the gas phase and in various solvents was presented by Robinson et al.[6]

Recently, we started a series of investigations of 5-substituted indoles with 5-methoxyindole,[7] 5-cyanoindole,[8] and 5-fluoroindole,[9] which will be continued with the present study. While 5-cyanoindole exerts a negative mesomeric effect (−M) on the chromophore and 5-fluoroindole a negative inductive effect (−I), the 5-substituent in 5-methoxy- and 5-hydroxyindole acts as +M effect substituent, increasing the electron density in the indole ring.

## 2. TECHNIQUES

**2.1. Experimental Procedures.** 5-Hydroxyindole (≥98%) was purchased from TCI and used without further purification. The experimental setup for the rotationally resolved laser induced fluorescence is described in detail elsewhere.[10] The laser system consists of a single frequency ring dye laser (Sirah Matisse DS) operated with Rhodamine 6G, pumped with 7 W of the 514 nm line of an $Ar^+$-ion laser (Coherent, Sabre 15 DBW). The dye laser output was coupled into an external folded ring cavity (Spectra Physics Wavetrain) for second harmonic generation. The resulting output power was constant at about 15 mW during the experiment. The molecular beam was formed by coexpanding 5OHI, heated to 210 °C, and 700 mbar of argon through a 200 $\mu$m nozzle into the vacuum chamber. The molecular beam passes two skimmers (1 mm and 3 mm, respectively) in a differentially pumped chamber in order to reduce the Doppler width. The resulting resolution is 18 MHz (fwhm) in this setup. In the third chamber, 360 mm downstream of the nozzle, the molecular beam crosses the laser beam at a right angle. The imaging optics setup consists of a concave mirror and two plano-convex lenses to focus the resulting fluorescence onto a photomultiplier tube, which is mounted perpendicularly to the plane defined by the laser and molecular beam. The signal output was then discriminated and digitized by a photon counter and transmitted to a PC for data recording and processing. The relative frequency was determined with a quasi confocal Fabry−Perot interferometer.

**Received:** May 2, 2012
**Revised:** June 28, 2012
**Published:** June 28, 2012

The absolute frequency was obtained by comparing the recorded spectrum to the tabulated lines in the iodine absorption spectrum.[11]

**2.2. Computational Methods.** *2.2.1. Quantum Chemical Calculations.* Structure optimizations were performed employing Dunning's correlation consistent polarized valence triple-$\zeta$ (cc-pVTZ) from the TURBOMOLE library.[12,13] The equilibrium geometries of the electronic ground and the lowest excited singlet states were optimized using the approximate coupled cluster singles and doubles model (CC2) employing the resolution-of-the-identity approximation (RI).[14−16] Vibrational frequencies and zero-point corrections to the adiabatic excitation energies have been obtained from numerical second derivatives using the NumForce script.[17] The transition state for the interchange of the *syn* and *anti* conformers in both electronic states was optimized using the Trust Radius Image Minimization (TRIM) algorithm,[18] implemented in the TURBOMOLE package, at the CC2/cc-pVTZ level of theory. A natural population analysis (NPA)[19] has been performed at the CC2 optimized geometries using the wave functions from the CC2 calculations as implemented in the Turbomole package.[17]

*2.2.2. Fits of the Rovibronic Spectra Using Evolutionary Algorithms.* We employed an evolutionary strategy (ES), namely, the covariance matrix adaptation ES (CMA-ES) for the fit of the rovibronic spectrum. This algorithm was developed by Ostermeier and Hansen.[20,21] It belongs, like the other search algorithms that are employed in our group, to the class of global optimizers that were inspired by evolutionary processes. For a detailed description of these evolutionary and genetic strategies for fitting of molecular spectra, we refer to refs 7 and 22.

## 3. RESULTS AND DISCUSSION

**3.1. High-Resolution Spectrum of the Origin Bands of 5-Hydroxyindole.** Figures 2 and 3 show the rotationally

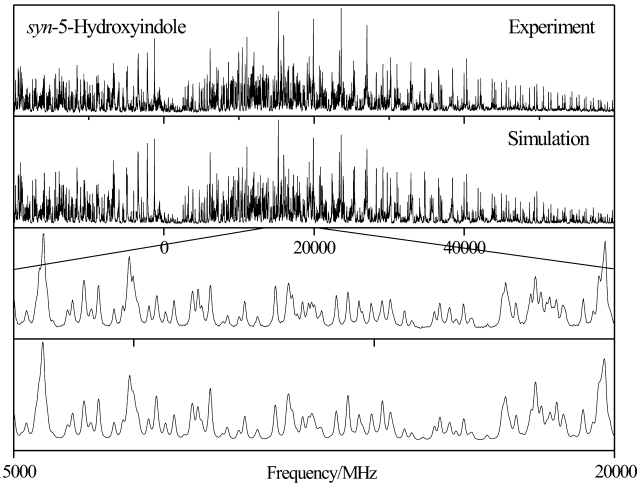


**Figure 2.** Rotationally resolved electronic spectrum of the electronic origin of *syn*-5-hydroxyindole.

resolved spectra of the two electronic origins A and B of 5OHI at 32 673.11 $cm^{-1}$ and 32 904.02 $cm^{-1}$. The experimental spectra could be simulated with a rigid rotor Hamiltonian including axis reorientation employing *ab*-type selection rules. The angles $\theta$ of the transition dipole moments with the inertial *a*-axes were determined to be 63° for the A band and 54° for the B band.

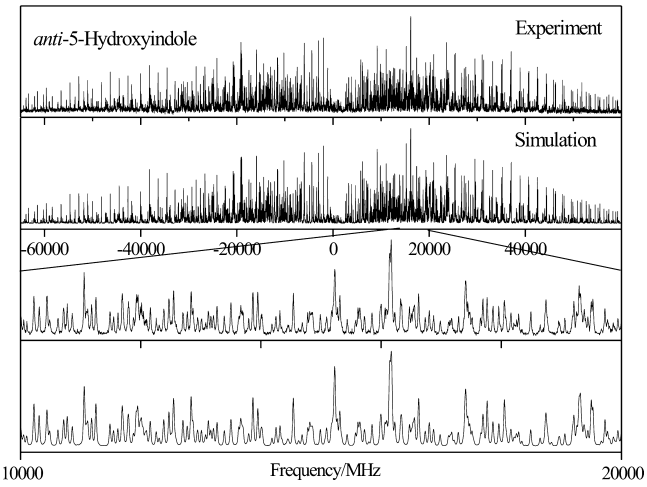


**Figure 3.** Rotationally resolved electronic spectrum of the electronic origin of *anti*-5-hydroxyindole.

Different thermalization of distinct $J_{K_AK_C}$ states of the molecules seeded in the molecular beam, requires a description of rotational state populations using several temperatures, which take the different rotational cooling into account. We use the two temperature model, proposed by Wu and Levy[23] with $n_i = e^{-E_i/kT_1} + we^{-E_i/kT_2}$, were $n_i$ is the population of the *i*th rovibronic level at energy $E_1$, $k$ is the Boltzmann constant, $T_1$ and $T_2$ are the two temperatures, and $w$ is a weighting factor modeling the contribution from $T_2$. The best agreement between experimental and simulated spectrum could be obtained with $T_1$ = 4.3 K, $T_2$ = 4.6 K, and $w$ = 0.05.

The zoomed details of both spectra show the excellent agreement between experiments and simulations, using the molecular parameters from the best fit employing the CMA-ES strategy, given in Table 1. The fit of the line shapes to Voigt profiles using a Gaussian (Doppler) contribution of 18 MHz yielded a Lorentzian contribution of 16 ± 1 MHz to the total line width for the A band and of 21 ± 1 MHz for the B band. These line widths are equivalent to an excited state lifetime of

**Table 1. CC2/cc-pVTZ Calculated Molecular Parameters of *syn*- and *anti*-5-Hydroxyindole and their Respective Experimental Values[a]**

| | CC2/cc-pVTZ | | exptl | |
|---|---|---|---|---|
| | syn | anti | band A | band B |
| $A''$ (MHz) | 3518 | 3526 | 3515.50(2) | 3522.79(2) |
| $B''$ (MHz) | 1043 | 1041 | 1041.35(1) | 1040.43(1) |
| $C''$ (MHz) | 804 | 804 | 803.67(1) | 803.51(1) |
| $\Delta I''$ (amu Å$^2$) | 0.0 | 0.0 | −0.22 | −0.24 |
| $A'$ (MHz) | 3399 | 3390 | 3393.56(2) | 3385.30(2) |
| $B'$/MHz | 1046 | 1046 | 1045.08(1) | 1045.99(1) |
| $C'$ (MHz) | 800 | 799 | 799.40(1) | 799.50(1) |
| $\Delta I'$ (amu Å$^2$) | 0.0 | 0.0 | −0.30 | −0.32 |
| $\Delta A$ (MHz) | −119 | −136 | −121.94(1) | −137.48(1) |
| $\Delta B$ (MHz) | +3 | +5 | +3.73(1) | +5.56(1) |
| $\Delta C$ (MHz) | −4 | −5 | −4.27(1) | −4.01(1) |
| $\theta$ (deg) | +70 | +66 | ±63 | ±54 |
| $\theta_T$ (deg) | +0.70 | +79 | ±0.53(6) | ±0.55(3) |
| $\nu_0$ ($cm^{-1}$) | 33207 | 33562 | 32673.11 | 32904.02 |

[a]Changes of the rotational constants are defined as $\Delta B_g = B'_g - B''_g$, with $B_g$ as rotational constants with respect to the inertial axes $g = a,b,c$.


dx.doi.org/10.1021/jp3042523 | J. Phys. Chem. A 2012, 116, 7873−7879

10 ± 0.5 ns for the A band and of 7.5 ± 0.5 ns for the B band. Huang and Sulkes reported values of 11.1 ns for both A and B bands from time-resolved spectroscopy.[2]

**3.2. Computational Results.** *3.2.1. Electronic Ground State.* The ground state structures of *syn*- and *anti*-5-hydroxyindole were optimized at the CC2/cc-pVTZ level of theory. At this level of theory (including zero-point energy corrections), the *anti* conformer is more stable by 155 $cm^{-1}$. The bond lengths of both conformers are given in Table 2, the

**Table 2. Bond Lengths (in pm) of *syn*- and *anti*-5OHI and Their Changes upon Electronic Excitation to the Lowest Singlet State from CC2/cc-pVTZ[a]**

| | $S_0$ | | $\Delta S_1$ | | $\Delta S_2$ | | $\Delta S_1$[21] |
|---|---|---|---|---|---|---|---|
| | *syn* | *anti* | *syn* | *anti* | *syn* | *anti* | indole |
| N1C2 | 137.7 | 137.7 | +4.1 | +4.1 | −3.9 | −4.2 | +4.0 |
| C2C3 | 137.7 | 137.8 | +0.7 | +0.3 | +5.7 | +6.0 | +0.6 |
| C3C9 | 142.9 | 142.9 | −0.2 | −0.1 | −2.5 | −2.4 | −0.2 |
| C9C4 | 140.4 | 140.7 | +0.5 | +0.0 | +2.8 | +2.8 | +0.6 |
| C4C5 | 138.7 | 138.7 | +3.8 | +4.5 | +2.6 | +3.2 | +4.6 |
| C5C6 | 141.0 | 141.0 | +2.3 | +0.6 | −0.8 | −1.5 | +1.5 |
| C6C7 | 139.0 | 138.9 | +3.6 | +4.0 | +5.3 | +5.6 | +3.9 |
| C7C8 | 139.5 | 139.7 | +1.6 | +1.4 | +1.5 | +0.8 | +1.2 |
| C8C9 | 142.3 | 142.1 | +2.7 | +3.3 | +0.4 | ±0.0 | +4.0 |
| C8N1 | 137.8 | 137.8 | −2.0 | −2.0 | +4.1 | +4.3 | −1.6 |
| N1H | 100.5 | 100.5 | +0.3 | +0.3 | +0.4 | +0.4 | +0.2 |
| C5O10 | 137.7 | 137.6 | −2.1 | −1.9 | +0.1 | +0.5 | |
| O10H11 | 96.4 | 96.5 | +0.6 | +0.4 | +0.1 | +0.1 | |

[a]For atomic numbering, cf. Figure 1.

rotational constants in Table 1 (Cartesian coordinates for all conformers and states can be found in the online Supporting Information). They are compared to the experimental rotational constants of the A and B bands of 5OHI. For the *anti* conformer, the calculated *A* rotational constant is 8 MHz larger than for *syn*-5OHI. We find exactly that difference for the *A* rotational constants of the B vs the A conformer. *B* and *C* rotational constants change by less than 1 MHz between the rotamers. From this difference, we make a preliminary assignment of band A being due to the *syn* conformer and of band B due to the *anti* conformer.

*3.2.2. Lowest Electronically Excited State.* The assignment of the origin bands to the rotamers based on the difference of the *A* rotational constant in the electronic ground state alone would not be very convincing, given its small value of only 8 MHz (only 0.2% of the absolute value). A second hint comes from the changes of the rotational constants upon electronic excitation. Here, we find a decrease of −119 MHz for the *syn* conformer, in very good agreement with the experimental value of −122 MHz for the A band, compared to −136 MHz for the *anti* conformer, which corresponds to an experimental value of −137 MHz for the B band. Thus, also the calculated geometry changes upon electronic excitation point to the assignment of band A to the *syn* conformer and of band B to the *anti* conformer.

The bond length changes upon electronic excitation to the lowest two excited singlet states in the two 5OHI conformers are compiled in Table 2 and are compared to those of indole. The strong decrease in C5O10 bond length upon excitation to the $S_1$ state points to a quinoidal structure in this excited state. In 5CI, the bond length between the C5 atom and the cyano group decreases by a comparable amount (−2.1 pm at SCS-CC2/cc-pVTZ level),[8] but the reason is quite different. The OH group donates electron density upon excitation, while the CN group is an electron acceptor. If one compares the geometry changes for the $S_1$ state of both 5OHI conformers with those of indole in Table 2, it is obvious, that the excited state geometry of the lowest excited singlet state of both conformers is $L_b$-like. It should be pointed out that, for molecules without at least $C_{2v}$ symmetry, the notations $L_a$ and $L_b$ are not based on symmetry arguments, and in fact, in the $C_s$ case, as for 5OHI, they belong to states with the same symmetry. These labels are merely a historic and convenient naming convention [22] to specify the lowest excited electronic states. Nevertheless, there are interesting differences in the excited state geometries of *syn*- and *anti*-5OHI. The most prominent differences are found with respect to bonds that play an important role in the coordinates that couple the $L_a$ and the $L_b$ states through a conical intersection (CI) in indole,[24] namely, C2C3, C4C9, and C4C5.

The electronic nature of the excited state can be deduced from the orientation of the transition dipole moment (TDM) in the molecular frame. For a planar molecule, the TDM orientation with respect to the inertial *a*-axis is defined via

$$\mu_a = \mu \cos\theta$$

Here, $\theta$ is the angle of the transition moment vector with the molecule fixed *a*-axis. The experimentally observed intensities of *a*- and *b*-type transitions in the electronic absorption spectrum are directly proportional to the squares of the projections of the TDM onto the inertial *a* and *b* axes. From these intensities, we deduced angles of the TDM with the *a*-axis of ±63° for the A- band (*syn*-5OHI) and of ±54° for the B band (*anti*-5OHI). One, however, cannot distinguish from the relative intensities of *a*- and *b*-lines alone between the two orientations of the TDM, which arise from the different signs of the TDM angle since they have the same projections onto the inertial axes.

As shown before, the relative sign of transition moment orientation and axis reorientation angle can be used to determine the absolute sign of $\theta$. We calculated the axis reorientation angle from the CC2/cc-pVTZ optimized geometries of the ground and excited state of both conformers, using the relationship first given by Hougen and Watson[25] for planar molecules using the Cartesian coordinates in the principal axis system of each state:

$$\tan(\theta_T) = \frac{\sum_i m_i(a'_i b''_i - b'_i a''_i)}{\sum_i m_i(a'_i a''_i + b'_i b''_i)} \quad (1)$$

Here, the doubly primed coordinates $a''_i$ and $b''_i$ refer to the coordinates of the *i*th atom in the principal axis system in the electronic ground state, the singly primed coordinates to the respective excited state coordinates, and $m_i$ is the atomic mass of the *i*th atom in the molecule. Using the CC2 optimized structures for the ground and excited states of both conformers, we obtain an axis reorientation angle of 0.70° for the *syn* conformer and of 0.79° for the *anti* conformer. We know from the fit of the intensities in the spectrum, that if $\theta_T$ is positive, then $\theta$ is necessarily positive and vice versa. Thus, the determination of the sign of $\theta_T$, which can be determined geometrically, provides a direct access to the absolute sign of $\theta$, which cannot be determined directly from the experiment since the observed intensities depend on the squares of the projections along the inertial axes as described above. The


dx.doi.org/10.1021/jp3042523 | J. Phys. Chem. A 2012, 116, 7873−7879

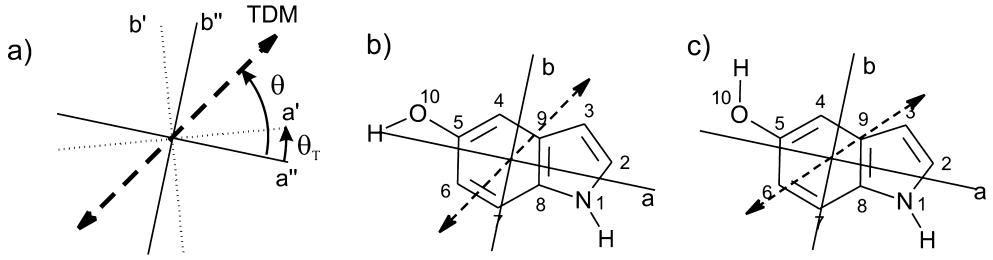


**Figure 4.** (a) Definition of the positive direction of the transition dipole moment angle $\theta$ and of the axis reorientation angle $\theta_T$. (b) TDM orientation in *syn*-5OHI. (c) TDM orientation in *anti*-5OHI.

positive direction of the angle $\theta$ is defined by a counterclockwise rotation of the inertial *a*-axis onto the TDM vector (cf. Figure 4), which corresponds to an $L_b$ state in Platts[26] nomenclature.

The quite large difference for the angles $\theta$ for both conformers cannot be traced back to a rotation of the inertial axes due to the rotation of the OH group. Figure 2 clearly shows that both axis systems are practically coincident due to the low mass of the hydrogen atom with respect to the rest of the molecule. It thus has to be a different electron density distribution in the two conformers, which is responsible for the different angles $\theta$.

Figure 5 shows the frontier orbitals of $\pi$-symmetry around the highest occupied molecular orbital (HOMO) and the lowest unoccupied molecular orbital (LUMO) of both conformers. Excitation to the $S_1$ state in the *syn* conformer has the following contributions, HOMO → LUMO (coefficient 0.93) and HOMO − 1 → LUMO + 5 (coefficient −0.27); while the *anti* conformer has the following contributions, HOMO → LUMO (coefficient 0.92) and HOMO − 1 → LUMO + 5 (coefficient +0.29). All molecular orbitals in between LUMO and LUMO + 5 are classified as Rydberg orbitals of $\sigma$ character, which are centered at the NH group of the pyrrole moiety, at the OH group in the 5-position, or at the CH groups. Excitation to the $S_2$ state has the largest coefficient for the HOMO − 1 → LUMO excitation, with smaller contributions from HOMO → LUMO + 5.

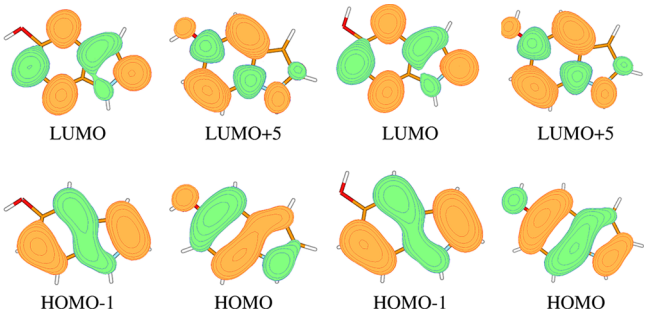


**Figure 5.** Contour plots of the highest occupied and lowest unoccupied molecular orbitals of *syn*- and *anti*-5OHI at the optimized $S_1$ geometry from CC2/cc-pVTZ calculations; isosurface value, 0.03.

Figure 6 presents the electron density difference plots upon excitation from the $S_0$ state to the lowest excited singlet state $S_1$ for both conformers. The differences between the density differences for both conformers are small in the chromophore, but since also a change of electron density in the OH bond is taking place upon excitation, the rotation of the TDM direction in the inertial axis system can be rationalized.

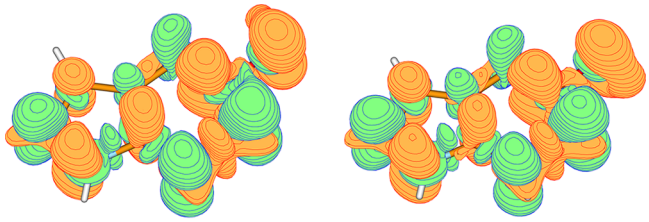


**Figure 6.** Isosurface plots of the density differences $\Delta\rho$ for *syn*- and *anti*-5OHI from the SCS-CC2/cc-pVTZ calculations; isosurface value, 0.001. Orange and green show regions of decreased and increased electron density, respectively.

Electronic excitation in indoles is generally accompanied by a shift of charge density from the benzene to the pyrrole ring. For both conformers, we calculated a shift of 0.06 elementary charges from benzene to pyrrole. However, the center of charges is different in both conformers. The carbon atom, in *ortho*-position with respect to the hydroxy group, bears a larger negative charge if the H-atom points toward it and a smaller if the H-atom of the hydroxy group points away from it. In a recent publication, we have shown how hyperconjugative effects influence the orientation of the TDM in different conformers.[27] In *syn*- and *anti*-5OHI, we can see the effect of the hyperconjugation between the $\sigma$-type binding orbital of the O-H bond with the $\sigma^*$ orbital of the CH bond in *ortho*-position, which gives rise to an increase of negative charge at the side, where the hyperconjugative effect takes place (Figure 7). Alternatively, the effect might be due to through space electrostatic interactions between the oxygen lone pairs and the respective neighboring C-atom.

*3.2.3. Higher Electronically Excited States.* The energetically following singlet state in the *anti* conformer is adiabatically located 3973 $cm^{-1}$ above the $L_b$ state and can be classified an as $L_a$ state. Its excitation is mainly HOMO → LUMO (coefficient 0.88) with smaller contributions from HOMO → LUMO + 5 (coefficient −0.22). The dipole moment and oscillator strength are considerably larger than the ones of the $S_1$ state. Also, the TDM orientation is in line with the assignment of the $S_2$ state being due to an $L_a$-type absorption. The adiabatic excitation energy of the *syn* conformer of the $S_2$ state is calculated to be 4440 $cm^{-1}$ higher than that of the $S_1$ state, with main contributions to the excitation being HOMO → LUMO (coefficient 0.83) and HOMO − 1 → LUMO (coefficient 0.35) (Table 3).

The excitation to the third excited singlet state in *syn*-5OHI comprises nearly equal contributions of HOMO → LUMO + 1 (coefficient 0.66) and HOMO → LUMO + 2 (coefficient 0.64). The first is a $\pi\sigma^*(NH)$ excitation, the second a $\pi\sigma^*(OH)$ excitation to Rydberg-like orbitals centered at the NH and at


dx.doi.org/10.1021/jp3042523 | J. Phys. Chem. A 2012, 116, 7873−7879

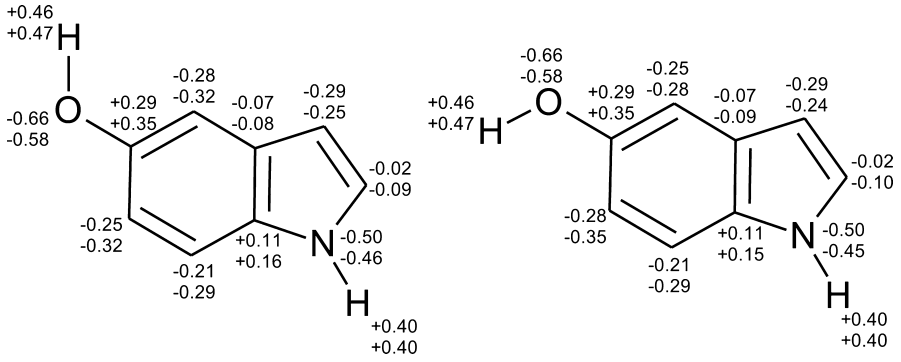


**Figure 7.** Natural charges from a natural population analysis (NPA) for *anti*- and *syn*-5OHI using the SCS-CC2/cc-pVTZ wave functions. The upper values give the $S_0$ charges, the lower values those of the $S_1$.

**Table 3. CC2 Calculated Properties of the Ground and Lowest Three Electronically Excited States of *syn*- and *anti*-5OHI[a]**

| | $S_0$ | | $S_1$ | | $S_2$ | | $S_3$ | |
|---|---|---|---|---|---|---|---|---|
| state | *syn* | *anti* | *syn* | *anti* | *syn* | *anti* | *syn* | *anti* |
| $\nu_0$ ($cm^{-1}$) | | | 33207 | 33562 | 37607 | 37535 | 49064 | 49228 |
| $f$ | | | 0.08 | 0.08 | 0.147 | 0.158 | 0.0001 | 0.0001 |
| $\theta$ | | | +70 | +66 | −6 | −15 | | |
| $\phi$ | | | +90 | +90 | +90 | +90 | 0 | 0 |
| $\mu$ (D) | 3.01 | 2.16 | 1.91 | 1.54 | 5.03 | 5.69 | 7.59 | 1.43 |

[a]Values for the $S_1$ and $S_2$ states are given at their respective minimum geometries. The $S_3$ is repulsive and calculated at the $S_0$ geometry.

the OH groups. The respective contributions in the *anti* conformer are HOMO − 1 → LUMO + 1 (coefficient 0.74) and HOMO → LUMO + 2 (coefficient 0.57). Both $\sigma$-type orbitals are shown in Figure 8.

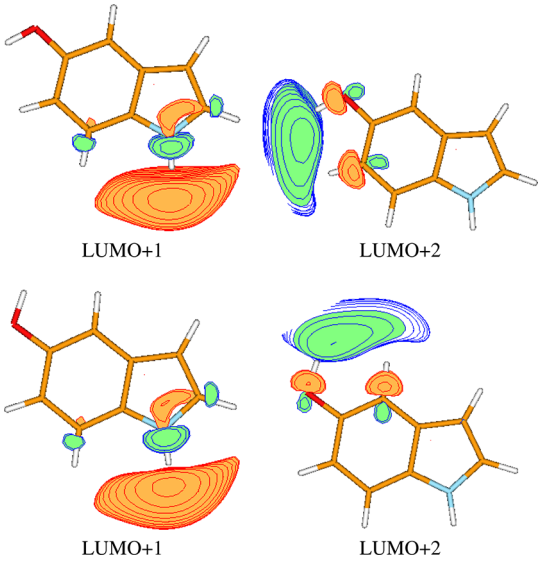


**Figure 8.** Contour plots of the two $\sigma^*$ orbitals of *syn*- (upper row) and *anti*-5OHI (lower row) at the optimized $S_0$ geometry from CC2/cc-pVTZ calculations; isosurface value, 0.03.

## 4. CONCLUSIONS

The electronic origin bands A and B of 5-hydroxyindole could be assigned to the *syn*- and *anti*-5OHI conformers on the basis of the rotational constants obtained from rotationally resolved electronic spectroscopy. CC2/cc-pVTZ calculations predict the *anti* conformer to be more stable by 155 $cm^{-1}$ than the *syn* conformer. This is the same energy order of conformers we found for *syn*- and *anti*-methoxyindole.[7] For this quite similar system, only the *anti* conformer could be observed experimentally. We repeated the ab initio calculations for the energy differences of the 5MOI conformers with the same method and basis set as in ref 7. The calculated energy difference between *syn*- and *anti*-5MOI amounts to 411 $cm^{-1}$. Although, this energy difference is nearly three times that of *syn*- and *anti*-5OHI, it is surprising, that no band in the electronic spectrum, due to the *syn* conformer could be observed for 5MOI, regarding the high temperature of the probe prior to expansion.

The barrier, which separates *syn*- and *anti*-5OHI, was calculated to be 973 $cm^{-1}$ in the electronic ground state and 3244 $cm^{-1}$ in the electronically excited state. These values are close to the $V_2$ barrier of the torsional motion of the hydroxy group in phenol.[28] The relative energies of the conformers and the barriers separating them are shown in Figure 9.

Since *anti*-5OHI is more stable in the electronic ground state, and the electronic origin frequency of the *anti*-conformer is shifted to higher energies relative to the *syn* conformer, the stabilities of both conformers must be reversed in the excited state.

While band A (due to the *syn* conformer) has an excited state lifetime of 10 ns, the lifetime of band B (the *anti* conformer) is only 7.5 ns. Regarding the fact that the chromophore is the same in both molecules, this finding is quite unexpected. Since both conformers exhibit bound potentials, tunneling between the minima cannot account for the different life times. A possible explanation might be different conical intersections with an unbound potential. Here, the most probable choice for this state is a $\pi\sigma^*$-type state with repulsive potential energy functions with respect to the stretching coordinates of OH or NH bonds.[29] A conical intersection (CI) along the OH coordinate seems to be the most probable candidate here since the position of the CI between the bound $\pi\pi^*$ state with the


dx.doi.org/10.1021/jp3042523 | J. Phys. Chem. A 2012, 116, 7873−7879

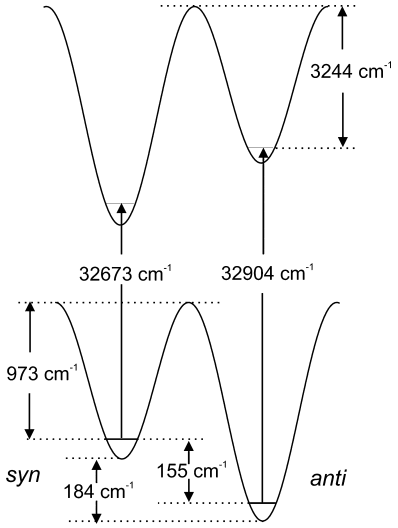


**Figure 9.** Schematic view of the relative energies of *syn*- and *anti*-5OHI in both electronic states and of the barriers, separating the minima at the potential energy surface (not drawn to scale).

repulsive $\pi\sigma^*$ state critically depends on the orientation of the group with respect to the chromophore. The sensitivity of the position of the conical intersection with respect to the vibrationless level of the primarily excited state has been shown in phenol, where the undeuterated isotopologue has a short lifetime of 2 ns, while deuterated phenol ($C_6H_5OD$) with lower zero-point energy has a considerably longer lifetime of 15 ns.[29,30] Vieuxmaire et al. discovered in phenol that the OH torsion, which interconverts the two conformers in 5OHI, is by far the strongest coupling mode for the CI between the $\pi\pi^*$ and the $\pi\sigma^*$ states.[31]

The transition moment orientations with respect to the inertial *a*-axes in the two conformers differ considerably by about 10°, which is confirmed by the CC2 calclations although the predicted difference is smaller by a factor of 2. We could perfectly reproduce the structures of both conformers in the ground and excited states and also the adiabatic excitation energy. Both theory and experiment agree that the observed state is an $L_b$ state, like in 5-fluoroindole, and contrary to 5-cyanoindole, where an $L_a$ state is observed. In both conformers of 5OHI, the $L_a$ state is the $S_2$, with considerably different rotational constants than the $L_b$ state.

The permanent dipole moment of the *syn* conformer is larger than that of the *anti* conformer, what can easily be understood from a simple vector addition of the main contribution to the dipole moment. In the *syn* conformer, the dipole vectors of the NH and the OH group point in the same direction, while they are nearly perpendicular in the *anti* conformer. In the $S_1$ state, the permanent dipole moment decreases for both conformers, relative to the ground state, with the *syn* dipole moment being the larger one. For the $S_2$, a considerably larger dipole moment is calculated as expected for an $L_a$ state. In this state, the order of dipole moments is reversed between the two conformers. The $S_3$ as the $\pi\pi^*$ state should have the highest dipole moment of all excited states. While this is fully confirmed for the *syn* conformer (7.59 D), the *anti* conformer has a surprisingly small permanent dipole moment of 1.43 D. Figure 8 reveals that the large dipole moments of the two $\sigma$ orbitals, which equally contribute to the transition, nearly cancel since they point in opposite directions.

## ■ ASSOCIATED CONTENT

### Supporting Information

CC2/cc-pVTZ calculated optimized Cartesian coordinates of both rotamers in the $S_0$, $S_1$, and $S_2$ states. This material is available free of charge via the Internet at http://pubs.acs.org.

## ■ AUTHOR INFORMATION

### Corresponding Author

*E-mail: mschmitt@uni-duesseldorf.de.

### Notes

The authors declare no competing financial interest.

## ■ ACKNOWLEDGMENTS

This work was financially supported by the Deutsche Forschungsgemeinschaft SCHM1043/11-1.

## ■ REFERENCES

(1) Arnold, S.; Sulkes, M. *Chem. Phys. Lett.* **1992**, *200*, 125−129.
(2) Huang, Y.; Sulkes, M. *Chem. Phys. Lett.* **1996**, *254*, 242−248.
(3) Livingstone, R.; Schalk, O.; Boguslavskiy, A. E.; Wu, G.; Bergendahl, L. T.; Stolow, A.; Paterson, M. J.; Townsend, D. *J. Chem. Phys.* **2011**, *135*, 194307.
(4) Oliver, T. A. A.; Kingz, G. A.; Ashfold, M. N. R. *Phys. Chem. Chem. Phys.* **2011**, *13*, 14646−14662.
(5) Catalán, J.; Pérez, P.; Acuña, A. U. *J. Mol. Struct.* **1986**, *42*, 179−182.
(6) Robinson, D.; Besley, N. A.; Lunt, E. A. M.; O'Shea, P.; Hirst, J. D. *J. Phys. Chem. B* **1986**, *113*, 2535−2541.
(7) Brand, C.; Oeltermann, O.; Pratt, D. W.; Weinkauf, R.; Meerts, W. L.; van der Zande, W.; Kleinermanns, K.; Schmitt, M. *J. Chem. Phys.* **2010**, *133*, 024303.
(8) Oeltermann, O.; Brand, C.; Engels, B.; Tatchen, J.; Schmitt, M. *Phys. Chem. Chem. Phys.* **2012**, *14*, 10266−10270.
(9) Brand, C.; Oeltermann, O.; Wilke, M.; Tatchen, J.; Schmitt, M. *ChemPhysChem* **2012**, DOI: 10.1002/cphc.201200345.
(10) Schmitt, M.; Küpper, J.; Spangenberg, D.; Westphal, A. *Chem. Phys.* **2000**, *254*, 349−361.
(11) Gerstenkorn, S.; Luc, P. *Atlas du spectre d'absorption de la molecule d'iode*; CNRS: Paris, 1982.
(12) Ahlrichs, R.; Bär, M.; Häser, M.; Horn, H.; Kölmel, C. *Chem. Phys. Lett.* **1989**, *162*, 165−169.
(13) Dunning, T. H., Jr. *J. Chem. Phys.* **1989**, *90*, 1007−1023.
(14) Hättig, C.; Weigend, F. *J. Chem. Phys.* **2000**, *113*, 5154−5161.
(15) Hättig, C.; Köhn, A. *J. Chem. Phys.* **2002**, *117*, 6939−6951.
(16) Hättig, C. *J. Chem. Phys.* **2002**, *118*, 7751−7761.
(17) *TURBOMOLE V6.1*; University of Karlsruhe and Forschungszentrum Karlsruhe GmbH: Karlsruhe, Germany, 2009; http://www.turbomole.com.
(18) Helgaker, T. *Chem. Phys. Lett.* **1991**, *182*, 503−510.
(19) Reed, A. E.; Weinstock, R. B.; Weinhold, F. *J. Chem. Phys.* **1985**, *83*, 735−746.
(20) Ostermeier, A.; Gawelczyk, A.; Hansen, N. *Lecture Notes in Computer Science: Parallel Problem Solving from Nature (PPSN III)*; Springer: New York, 1994; pp 189−198.
(21) Hansen, N.; Ostermeier, A. *Evol. Comput.* **2001**, *9* (2), 159−195.
(22) Meerts, W. L.; Schmitt, M. *Int. Rev. Phys. Chem.* **2006**, *25*, 353−406.
(23) Wu, Y. R.; Levy, D. H. *J. Chem. Phys.* **1989**, *91*, 5278−5284.
(24) Brand, C.; Küpper, J.; Pratt, D. W.; Meerts, W. L.; Krügler, D.; Tatchen, J.; Schmitt, M. *Phys. Chem. Chem. Phys.* **2010**, *12*, 4968−4997.
(25) Hougen, J. T.; Watson, J. K. G. *Can. J. Phys.* **1965**, *43*, 298−320.
(26) Platt, J. R. *J. Chem. Phys.* **1949**, *17*, 484−495.
(27) Brand, C.; Meerts, W. L.; Schmitt, M. *J. Phys. Chem. A* **2011**, *115*, 9612−9619.
(28) Berden, G.; Meerts, W. L.; Schmitt, M.; Kleinermanns, K. *J. Chem. Phys.* **1996**, *104*, 972−982.

(29) Sobolewski, A. L.; Domcke, W.; Dedonder-Lardeux, C.; Jouvet, C. *Phys. Chem. Chem. Phys.* **2002**, *4*, 1093−1100.
(30) Ratzer, C.; Küpper, J.; Spangenberg, D.; Schmitt, M. *Chem. Phys.* **2002**, *283*, 153−169.
(31) Vieuxmaire, O. P. J.; Lan, Z.; Sobolewski, A. L.; Domcke, W. *J. Chem. Phys.* **2008**, *129*, 224307.